materials

MDPI

Article

A New Creep–Fatigue Interaction Model for Predicting Deformation of Coarse-Grained Soil

Jie Zhang, Qiuhua Rao * and Wei Yi

School of Civil Engineering, Central South University, Changsha 410075, China; jinxi625@live.cn (J.Z.); yi.wei@csu.edu.cn (W.Y.)
* Correspondence: raoqh@csu.edu.cn

Abstract: Studying the creep–fatigue interaction of the coarse-grained soil (CGS) is very important for safety assessment and disaster prevention in subgrade engineering. Current research work is mainly focused on single creep or fatigue deformation. In this paper, a new creep–fatigue interaction model is established to predict the creep–fatigue interaction deformation of different gradation CGS based on the rheological mechanics and the interactive relationship between creep and fatigue complex compliance method. Triaxial creep–fatigue interaction tests of different gradations CGS under different average stresses and frequencies were conducted to verify the new creep–fatigue interaction model. Research results show that for the creep–fatigue and fatigue–creep interaction, the fatigue deformation is always larger than the creep deformation under the same stress level. For the creep–fatigue multi-interaction, the second creep and fatigue deformation are always smaller than the first creep and fatigue deformation. The results of the triaxial creep–fatigue interaction tests verify the validity of this new model.

Keywords: creep–fatigue interaction; coarse-grained soil; rheological mechanic; creep–fatigue interaction test; nonlinear regression

Citation: Zhang, J.; Rao, Q.; Yi, W. A New Creep–Fatigue Interaction Model for Predicting Deformation of Coarse-Grained Soil. *Materials* **2022**, *15*, 3904. https://doi.org/10.3390/ma15113904

Academic Editors: Cesare Oliviero Rossi, Pietro Calandra, Evangelos J. Sapountzakis, Bagdat Teltayev, Paolino Caputo, Valeria Loise and Michele Porto

Received: 14 April 2022
Accepted: 29 May 2022
Published: 30 May 2022

1. Introduction

Coarse-grained soil (CGS in short) is a mixture of pebble, sand and clay, etc. [1,2], and is commonly used as a subgrade material in highway and railway engineering [3–5]. It is generally subjected to static or repeated dynamic load caused by transportation tools (vehicles and trains) [6,7]. Since pebble and sand usually show elasticity while clay has viscoelasticity, the CGS is considered to be of rheological properties [8]. Under long-term static–dynamic (i.e., creep–fatigue) interaction loading, the CGS may cause uneven settlement and potential safety hazards for the highway and railway [9].

Currently, there are two main creep–fatigue loading forms: the simultaneous superposition of creep and fatigue loads [10,11] and alternative creep and fatigue loads [12,13], among which the latter is a common case for the CGS of subgrade in highway and railway engineering since the vehicles and trains usually have an alternative state of stopping or moving (i.e., successive creep–fatigue loads). Therefore, it is of great significance to study the successive creep–fatigue interacting models and mechanisms for predicting the long-term deformation of CGS. Niya Dong [14] proposed a newly modified multi-sequenced repeated load test, measured the strain, resilient modulus, and creep compliance, proposed new factors to evaluate the viscoelasticity of different asphalt mixtures. V. P. Golub [15] proved that there exists a definite correlation between the processes of static and cyclic creep and proposed a relationship of creep–fatigue interaction. Yunliang Li [16] analyzed the cement emulsified asphalt composite binder evolution process of fatigue damage by fatigue test, and with the increase in fatigue damage, instantaneous elastic deformation and creep rate increase in steady creep stage during creep process. Linjian Ma [13] conducted the creep–fatigue interaction test of rock salt by trapezoidal wave, and the

results showed that under combined creep and fatigue, the cycling life of the rock salt is remarkably lower compared with that observed in pure fatigue or creep tests and the life of creep–fatigue interaction can be alternatively predicted without rupturing the salt specimens. Hongfu Liu [11] established a fatigue–creep damage interaction model considering the interaction of fatigue and creep damage based on the principle of semi-sine fatigue stress decomposition. The results indicated that the damage of the asphalt mixture under the action of the semi-sine cyclic load was not a simple linear accumulation of fatigue damage and creep damage, but an overall result of the interaction of fatigue damage, creep damage, and fatigue–creep damage. Qian Li [17] researched and indicated that cyclic loading has a significant influence on the creep of high-strength high-performance concrete, especially during the early stage of creep development. Additionally, the modified creep model can be adopted to predict the long-term behaviors of concrete bridges, which are always subjected to cyclic traffic loading. Bara Wasfi Al-Mistarehi [18] considered that the accumulated strain which increased with time at different levels of temperature for all types of fillers was obtained from the creep test and fatigue test and between logarithm strain and logarithm number of cycles. As a result, the waste toner as filler was the best filler. Rafiqul Tarefder [19] showed that the increase in freeze–thaw cycles in asphalt concrete decreased the indirect tensile strength and tensile strength ratio of asphalt. Xiaozhao Li [20] proposed an analytical solution by coupling the confined cyclic static loading and unloading path, the Hooke–Kelvin viscoelastic model and the formulated micro–macro model which explains the total time-dependent visco–elastic–plastic deformation caused by the microcracks variable during cyclic static compressive failure. Vitaliy M. Kindrachuk [21] developed a fatigue model for normal strength concrete under compressive loading conditions based on continuum damage mechanics which incorporates creep and fatigue phenomena in a single framework and postulates damage to be driven by inelastic deformations. Yu Su [5] developed a fatigue model of railway soil that considered the coarse grain content and the number of loading cycles. Abdulgazi Gedik [22] studied the fatigue and dynamic creep modulus of asphalt pavement with recycling fluorescent lamps and Yasser M [23] studied the dynamic rheological characteristics of asphalt pavement with two different recycled plastic wastes. Estelle Delfosse Ribay [24] presented the creep and fatigue behaviors of grouted sand to analyze the strain rate, creep slope or fatigue slope, and the creep limit strength or fatigue limit strength. Alireza Ameli [25] analyzed the resilient modulus, indirect tensile strength and dynamic creep of asphalt binders and mixtures. Very few studies are available on the creep–fatigue interaction of the CGS.

In this paper, two new interaction parameters are proposed to establish the new creep–fatigue interaction model based on rheology mechanics and the relationship between the creep and fatigue complex compliance. The interaction parameters were determined by the triaxial creep and fatigue tests, and the new interaction model was verified by the predicted and tested results of the triaxial creep–fatigue interaction tests.

2. Establishment of New Creep–Fatigue Interaction Model

2.1. Definition of the New Creep–Fatigue Interaction Factor

Figure 1 shows the creep–fatigue interaction process of the CGS under triaxial compression ($\sigma_1 > \sigma_3$, σ_1 and σ_3 are axial and confining stresses), where the interaction order can be the creep first followed by fatigue (creep–fatigue interaction, C-F for short), or the fatigue first followed by creep (fatigue–creep interaction, F–C in short). For each creep–fatigue interaction process, the creep stress ($\sigma_1 = \sigma_c$, σ_c is the creep stress, $\sigma_c - \sigma_3$ is the deviatoric stress of creep) is applied to the CGS for a period of time ($t = t_1$) and unloaded to be $\sigma_1 = \sigma_3$, and then the fatigue stress in terms of semi-sine ($\sigma_1 = \sigma_f = 2\sigma_c|sin\omega t|$, ω is circular frequency, $\omega = 2\pi f$, f is fatigue loading frequency) is applied to the CGS for a period of time ($t = t_2 - t_1$). Let the creep deviatoric stress ($\sigma_c - \sigma_3$) be equal to the average deviatoric

stress of the fatigue cycle ($\sigma_a = \sigma_c - \sigma_3$, σ_a is the average deviatoric stress of fatigue, $\sigma_a = (\sigma_f - \sigma_3)/2$) since in order to establish a relationship under the same stress factor.

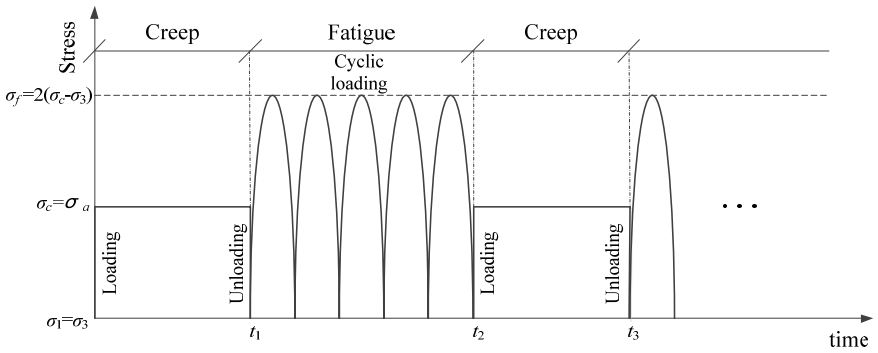

Figure 1. The process of creep–fatigue interaction.

In order to study the creep–fatigue interaction for the CGS deformation, it is necessary to seek a creep–fatigue interaction parameter to link up the two loading processes.

In rheologic mechanics, there exists a relationship of Fourier equivalent transformation between the creep compliance $J(t)$ and fatigue compliance $J(\omega)$, where $\mathcal{F}$ is Fourier transformation and $\mathcal{F}^{-1}$ is inverse Fourier transformation.

$$\begin{aligned} J(\omega) &= \mathcal{F}[J(t)] \\ J(t) &= \mathcal{F}^{-1}[J(\omega)] \end{aligned} \tag{1}$$

Since test results show that the CGS has larger fatigue deformation than creep deformation under $\sigma_a = \sigma_c$ [26], $J(t)$ and $J(\omega)$ cannot be equivalently transformed by Equation (1). For modifying Equation (1) to obtain the actual equivalent transform relationship between $J(t)$ and $J(\omega)$ of the CGS, $J(\omega)$ is divided into a real part $J_r(\omega)$ and imaginary part $J_i(\omega)$, and $J(t)$ can also be in terms of its real part $J_r(t)$ and imaginary part $J_i(t)$ by Fourier transform.

$$\begin{aligned} J_r(t) &= \omega\int_0^\infty J(t)\sin\omega t dt \\ J_i(t) &= \omega\int_0^\infty J(t)\cos\omega t dt \end{aligned} \tag{2}$$

Considering that both the creep and fatigue compliances have real and imaginary parts, define two new creep–fatigue interaction factors k and g, define the matrices $A_{1\times2} = (J_r(t)\ J_i(t))$, $B_{1\times2} = (J_r(\omega)\ J_i(\omega))$ and $M_{2\times2} = \begin{pmatrix} k & 0 \\ 0 & g \end{pmatrix}$, and then establish the relationship between the real and imaginary parts of the creep ($J_r(t)$, $J_i(t)$) and fatigue ($J_r(\omega)$, $J_i(\omega)$) compliances, i.e., the new creep–fatigue interaction model:

$$\begin{aligned} \begin{pmatrix} J_r(t) & J_i(t) \end{pmatrix}\begin{pmatrix} k & 0 \\ 0 & g \end{pmatrix} &= \begin{pmatrix} J_r(\omega) & J_i(\omega) \end{pmatrix} \\ \begin{pmatrix} J_r(\omega) & J_i(\omega) \end{pmatrix}\begin{pmatrix} k & 0 \\ 0 & g \end{pmatrix}^{-1} &= \begin{pmatrix} J_r(t) & J_i(t) \end{pmatrix} \end{aligned} \tag{3}$$

For simplifying the expression, that is Equation (5):

$$\begin{aligned} AM &= B \\ BM^{-1} &= A \end{aligned} \tag{4}$$

Since $J_r(t)$, $J_i(t)$ and $J_r(\omega)$, $J_i(\omega)$) are obtained by the following creep and fatigue tests, respectively, k and g can be calculated by Equation (4).

2.2. Determination of Creep–Fatigue Interaction Factor

In order to determine the creep–fatigue interaction parameters k and g: (1) conduct the triaxial creep tests (creep stress σ_c) and the fatigue tests (fatigue average stress σ_a) under the same average stress condition ($\sigma_c - \sigma_3 = \sigma_a$) to determine creep compliance and fatigue compliance; (2) calculate the creep and fatigue real and imaginary parts of compliance; and (3) compare the real parts and imaginary parts of the creep and fatigue compliance to determine the k and g.

2.2.1. Scheme of Triaxial Creep and Fatigue Tests

According to the Code for the Design on Subgrade of Railway in China (TB10001-2005), three different gradations of CGS were prepared by different mass ratios of pebble (γ) (with high elastic modulus), sand and clay (with rheological properties), as listed in Table 1. Figures 2 and 3 showed their grain–size distribution curves and water content (w)–dry density (ρ_d) curves for three different gradations of CGS, respectively. The CGS specimens are cylinders of Φ300 mm × 600 mm and prepared by the layered compacting method (Figure 4).

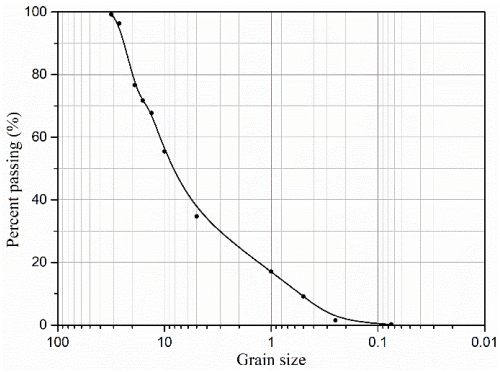

(**a**)

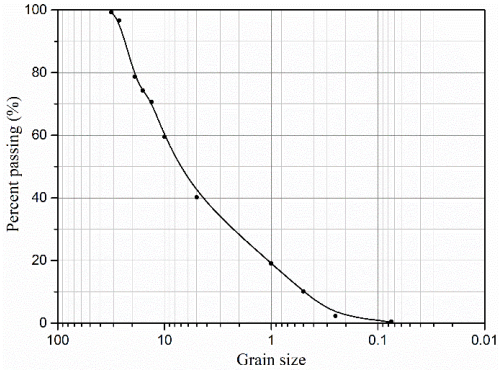

(**b**)

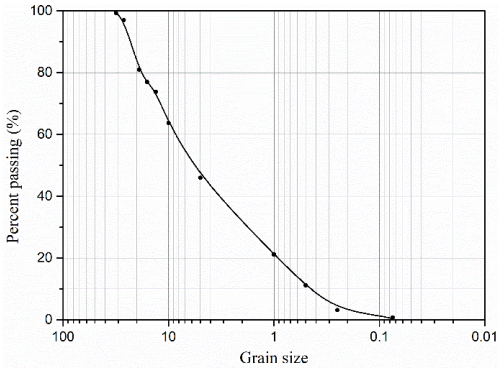

(**c**)

Figure 2. Grain–size distributions curves for three different gradations of CGS: (**a**) S1; (**b**) S2; and (**c**) S3.

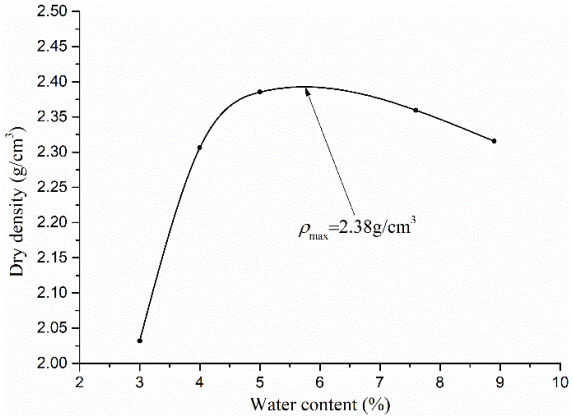

(**a**)

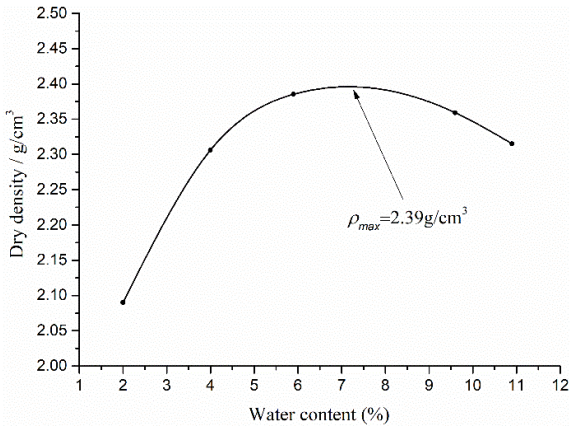

(**b**)

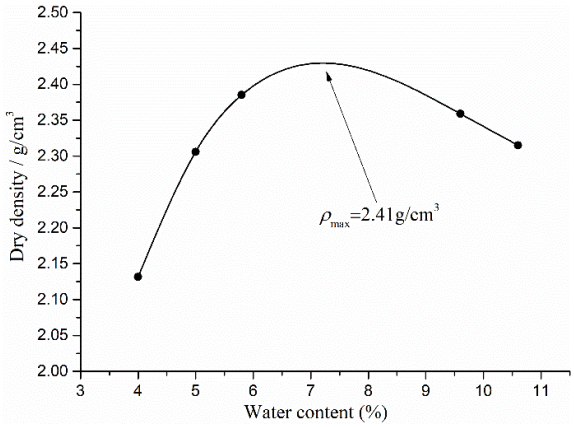

(**c**)

Figure 3. Water content–dry density curves for three different gradations of CGS: (**a**) S1; (**b**) S2; and (**c**) S3.

Figure 4. Cylindric specimen of CGS.

Table 1. Three different mass ratios of CGS.

No.	Pebble (γ)	Sand	Clay
S1	1	1	0.30
S2	1	1	0.75
S3	1	1	1.33

Triaxial compressive creep and fatigue tests were conducted on the TAJ-2000 triaxial testing system (Figure 5). Table 2 lists their loading conditions for the three different gradations of CGS specimens, where the confining pressure σ_3 was 0.2 MPa ($\sigma_3 < \sigma_1$). Let the average stress of fatigue test $\sigma_a = \sigma_c - \sigma_3$. There were a total of 9 creep tests (3 specimen × 3 stress) and 27 fatigue tests (3 specimen × 3 stress × 3 frequency). For each test, three identical specimens were prepared and there were 108 specimens in total. During the creep tests, the strain was recorded every 2 min to obtain the creep curves. During the fatigue tests, the strain and stress were recorded 10 times in one cycle.

Figure 5. TAJ-2000 triaxial testing system.

Table 2. Loading conditions for the triaxial compressive creep and fatigue tests (σ_3 = 0.2 MPa).

No.	Creep		Fatigue			
	σ_c/MPa	Holding Time *t*/min	Peak Stress σ_f /MPa	Frequency *f*/Hz	Cycle Number num/N	Average Stress σ_a/MPa
S1/S2/S3	0.3	120	0.4	1	7200	0.1
				2	14,400	
				3	21,600	
	0.4		0.6	1	7200	0.2
				2	14,400	
				3	21,600	
	0.5		0.8	1	7200	0.3
				2	14,400	
				3	21,600	

2.2.2. Triaxial Creep Test and Analyses

(1) Creep parameters under different stress

In this study, the Burgers creep model (Figure 6, Equation (5)) was adopted to describe the creep phenomenon of the different gradations of CGS and the creep compliance $J(t)$ can be obtained by fitting the tested creep curves:

$$J(t) = \frac{1}{E_1} + \frac{t}{\eta_1} + \frac{1 - e^{-\frac{tE_2}{\eta_2}}}{E_2} \quad (5)$$

where E_1, E_2, η_1, η_2 are creep parameters of the Burgers model.

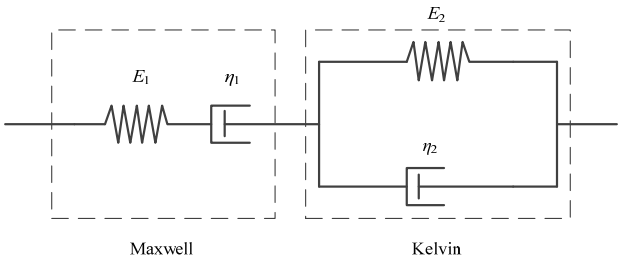

Figure 6. Burgers model.

Figure 7 shows the tested creep strain data (ε_c) under different time (t) curves for different constant stress (σ_c = 0.3 Mpa, 0.4 Mpa, 0.5 Mpa) for the CGS specimens of three different gradations, as well as their fitted curves by the Burgers creep model (Equation (14)). Table 3 lists the fitted Burgers model parameters with high fitting precision (R^2 > 0.995). It is seen that all the creep curves have three stages: the instantaneous deformation stage (t = 0), attenuation deformation stage (with decreasing slope), and stable creep deformation stage (with a constant slope). Obviously, for the same gradation of the CGS specimen, ε_c is increased with the increase in σ_c. While for the different gradations of the CGS specimen, ε_c is increased with the decrease in pebble content γ since a smaller γ means more clay content with stronger rheological properties.

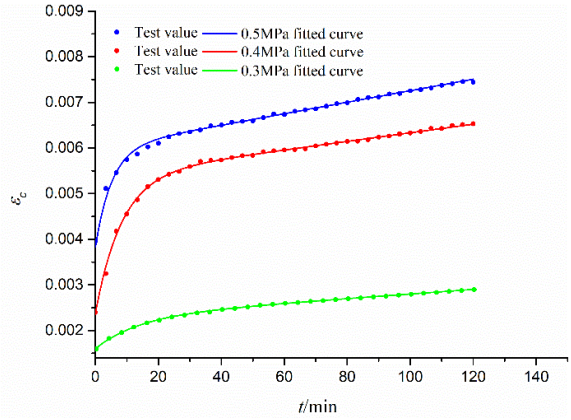

(**a**)

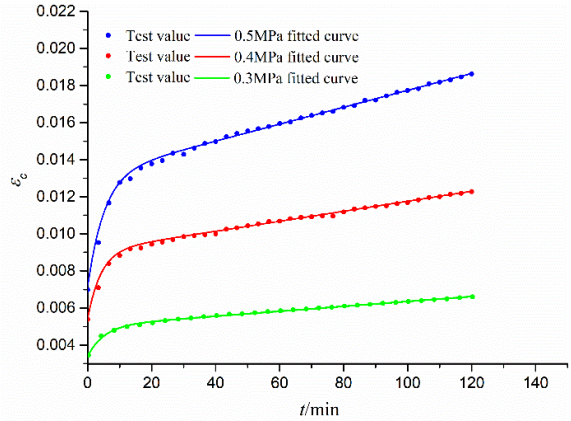

(**b**)

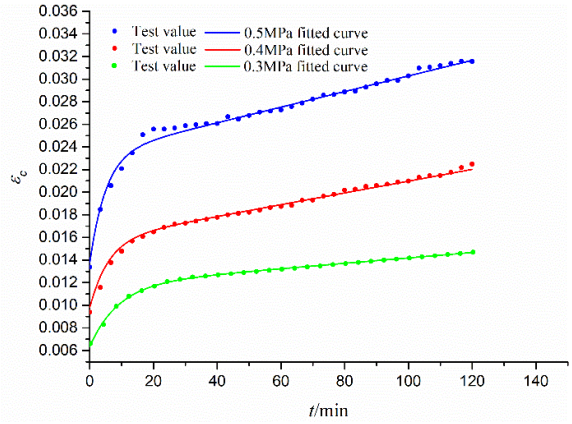

(**c**)

Figure 7. Creep curves for different gradations of CGS specimens: (**a**) S1; (**b**) S2; and (**c**) S3.

Table 3. Burgers model parameters for different gradations of CGS.

No.	$\sigma_c - \sigma_3$/MPa	E_1/MPa	E_2/MPa	η_1/MPa·min	η_2/MPa·min	R^2
S1	0.1	62.51	142.95	19,958.67	1974.63	0.997
	0.2	83.33	66.67	21,276.59	555.56	0.998
	0.3	78.13	138.88	23,809.52	730.99	0.996
S2	0.1	29.36	61.22	7544.07	312.03	0.998
	0.2	36.49	55.56	7407.40	229.56	0.996
	0.3	41.67	50.00	6578.94	257.73	0.996
S3	0.1	15.74	18.33	4196.82	163.64	0.998
	0.2	20.28	33.67	3846.15	199.23	0.997
	0.3	21.73	31.25	4347.82	157.82	0.995

(2) Unified creep parameters for different creep stresses and gradations

It was found in Table 3 that the Burgers creep parameters depend not only on the creep stress (σ_c) or the deviatoric stress ($\sigma = \sigma_c - \sigma_3$), but also on the gradations (mass ratios γ, water content w). In order to obtain a unified creep parameter relationship (related to σ, γ, and w) to describe the creep behaviors for different gradations of CGS under different stresses, the nonlinear regression is needed. Since the Burgers model (Figure 6) is the Maxwell model connected to the Kelvin model in series, E_1 and η_1 are independent parameters, while E_2 and η_2 are coupling parameters. Therefore, the unified creep parameter relationship can be determined by nonlinear regression with high precision ($R^2 > 0.989$).

$$\begin{aligned}
\lg(E_1) &= 0.943 + 0.648\sigma - 2.844\gamma - 7.609w \quad (R^2 = 0.989)\\
\lg(\eta_1) &= 4.486 + 0.054\sigma - 2.321\gamma - 20.318w \quad (R^2 = 0.992)\\
\lg(E_2) &= -0.106 + 0.057\sigma + 0.299\gamma + 3.189w + 0.472\lg(\eta_2)\\
&\quad - 0.211\lg^2(\eta_2) + 0.377\lg(E_2)\lg(\eta_2) \quad (R^2 = 0.998)\\
\lg(\eta_2) &= 1.660 - 0.097\sigma - 0.328\gamma - 2.255w - 0.156\lg(E_2)\\
&\quad - 0.265\lg^2(E_2) + 0.451\lg(E_2)\lg(\eta_2) \quad (R^2 = 0.999)
\end{aligned} \tag{6}$$

Table 4 lists the nonlinearly regressed and tested values of Burgers creep parameters for comparison. They fit well, mostly with the error $E < 10\%$, which proves the validity of Equation (6). Based on Burgers creep model and its parameter (Table 4), Figure 8 gives the tested and nonlinearly regressed creep curves (ε_c–t) under different creep stresses for three

gradations of CGS. It is seen that they are almost the same at the instantaneous deformation stage. In the attenuation deformation stage, their differences increase with time but tend to be unchanged in the stable deformation stage. In a word, they are approximately close to each other, which again proves the validity of Equation (6).

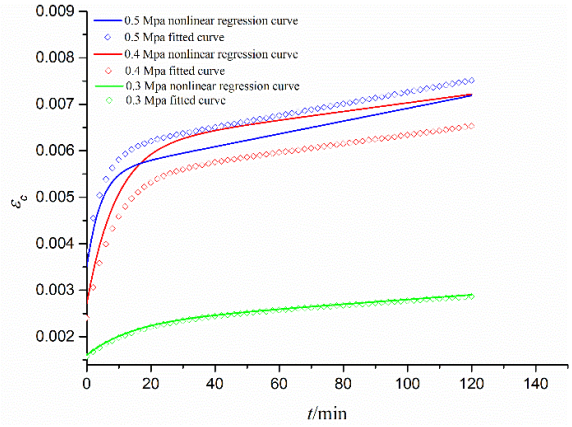

(**a**)

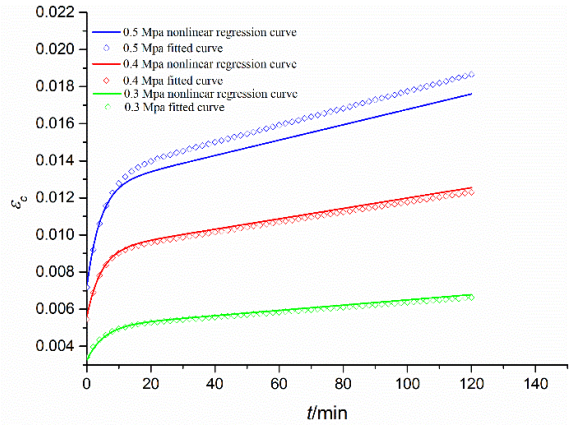

(**b**)

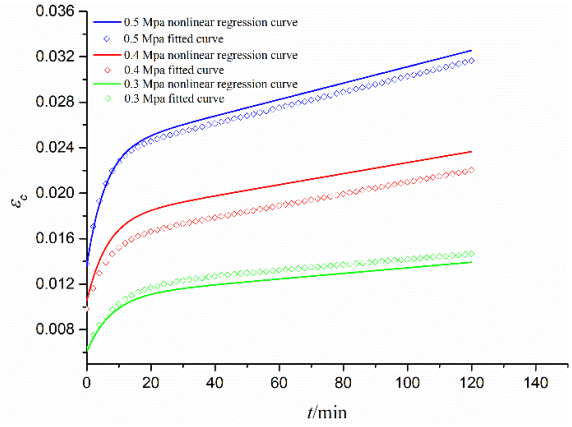

(**c**)

Figure 8. Fitted and nonlinearly regressed creep curves under different stresses for different gradations of CGS: (**a**) S1; (**b**) S2; and (**c**) S3.

Table 4. Regressed and tested values of Burgers creep parameters.

No.		S1			S2			S3		
σ_c/MPa		0.3	0.4	0.5	0.3	0.4	0.5	0.3	0.4	0.5
E_1/MPa	Tested value	62.51	83.33	78.13	29.36	36.49	41.67	15.74	20.28	21.73
	Calculated value	63.65	73.89	85.78	30.47	35.37	41.07	16.38	19.02	22.08
	Error	1.82%	11.32%	9.79%	3.78%	3.06%	0.05%	4.06%	6.21%	1.61%
E_2/MPa	Tested value	142.95	66.67	138.88	61.22	55.56	50.00	18.33	33.67	31.25
	Calculated value	138.02	58.88	146.98	54.95	56.23	57.07	20.41	27.28	28.96
	Error	3.44%	11.68%	5.81%	10.24%	1.21%	14.14%	11.34%	18.90%	7.32%
η_1/MPa·min	Tested value	19,958.67	21,276.59	23,809.52	7544.07	7407.40	6578.94	4196.82	3846.15	4347.82
	Calculated value	21,300.86	21,567.37	21,837.21	7057.92	7146.23	7235.64	4064.62	4115.48	4166.97
	Error	6.72%	1.36%	8.28%	6.44%	3.52%	9.98%	3.15%	7.00%	4.15%
η_2/MPa·min	Tested value	1974.63	555.56	730.99	312.03	229.56	257.73	163.64	199.23	157.82
	Calculated value	2092.09	531.02	630.95	293.26	251.18	239.88	158.48	176.42	165.95
	Error	5.94%	4.41%	13.68%	6.01%	9.41%	6.92%	3.15%	11.44%	5.15%

2.2.3. Triaxial Fatigue Test and Analyze

(1) Fatigue compliance formulae

When the sine wave is adopted as the fatigue load:

$$\sigma = \sigma_f \sin \omega t \tag{7}$$

The strain response is

$$\begin{aligned} \varepsilon &= \varepsilon_f \sin(\omega t - \delta) \\ \varepsilon_f &= \sigma_f \left| J(\omega) \right| \end{aligned} \tag{8}$$

where σ_f and ε_f are the peak stress and strain of fatigue, δ is the phase angle and $|J(\omega)|$ is the module of fatigue compliance.

Equations (7) and (8) can be rewritten as

$$\frac{\sigma}{\sigma_f} = \sin \omega t \tag{9}$$

$$\frac{\varepsilon}{\varepsilon_f} = \sin \omega t \cos \delta - \sqrt{1 - \sin^2 \omega t} \sin \delta \tag{10}$$

Substituting Equation (9) into Equation (10) yields the strain–stress relationship, i.e., the elliptic Equation:

$$\frac{\sigma^2}{\sigma_f^2} + \frac{\varepsilon^2}{\varepsilon_f^2} - \frac{2 \cos \delta}{\sigma_f \varepsilon_f} \sigma \varepsilon - \sin^2 \delta = 0 \tag{11}$$

Since this elliptic Equation is obtained by fitting the data of a one-cycle fatigue test, the phase angle δ can be determined by Equation (11).

Therefore, the real parts $J_r(\omega)$ and imaginary parts $J_i(\omega)$ of the fatigue compliance can be calculated by Equation (8) and the relationship of the phase angle δ and the fatigue compliance [23] are as follows:

$$\begin{aligned} \tan\delta &= \frac{J_i(\omega)}{J_r(\omega)} \\ \left|J(\omega)\right| &= \sqrt{J_r(\omega)^2 + J_i(\omega)^2} \end{aligned} \tag{12}$$

(2) Experimental determination of fatigue compliance

Dynamic loading adopts the stress-controlled cyclic loading method, applying semi-sine wave axial cyclic stress, and the fatigue load was applied on the specimen after the balance of $\sigma_1 = \sigma_3$, and recorded 10 points of the stress and strain in one cycle by the test system. Figure 9 shows some specimens after the fatigue test of different gradations of CGS.

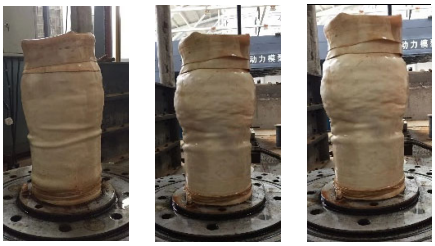

(**a**) (**b**) (**c**)

Figure 9. Deformation of CGS after fatigue tests: (**a**) S1; (**b**) S2; and (**c**) S3.

Figures 10 and 11 show the tested and fitted hysteretic curves of the S1 specimen (at different frequency f for the same average stress σ_a) and the S2 specimen (under different σ_a for the same *f*) for a one-cycle load for example. Table 5 lists the areas of the hysteretic circles (*A* represents the energy dissipation in one cycle, Equation (13) [27]) obtained by Matlab with its own written code. It can be seen that *A* slightly decreased with the increase in *f*, that is, the frequency effect is much smaller, while *A* was almost multiplied as it increased with the multiplied increasing of σ_a for the same gradation CGS. Additionally, *A* increased with the decrease in pebble content (γ) for different gradations of CGS, because a greater γ means that the CGS specimen had weaker rheological properties; therefore, the smaller γ represents the stronger rheological properties which could dissipate more energy in one cycle. The fatigue compliance ($J_r(\omega)$, $J_i(\omega)$, $J(\omega)$ and δ) can be calculated by Equations (7)–(13).

$$\begin{aligned} A &= \pi\sigma_f\varepsilon_f \sin\delta \\ &= \pi\sigma_f^2 J_i(\omega) \end{aligned} \tag{13}$$

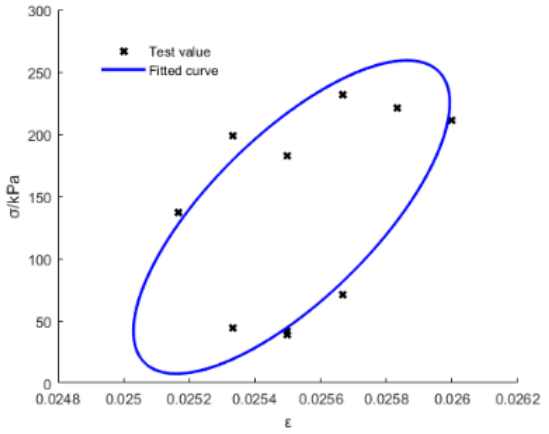

(**a**)

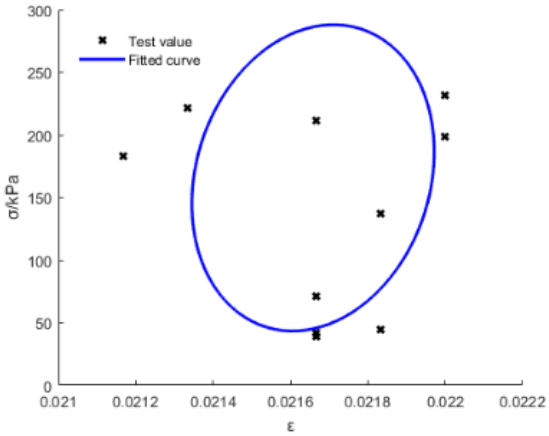

(**b**)

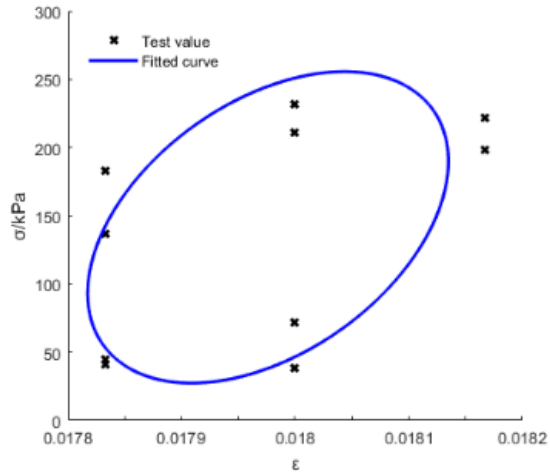

(**c**)

Figure 10. Tested and fitted hysteretic curves of the S1 specimen under different frequencies: (**a**) 1 Hz; (**b**) 2 Hz; and (**c**) 3 Hz.

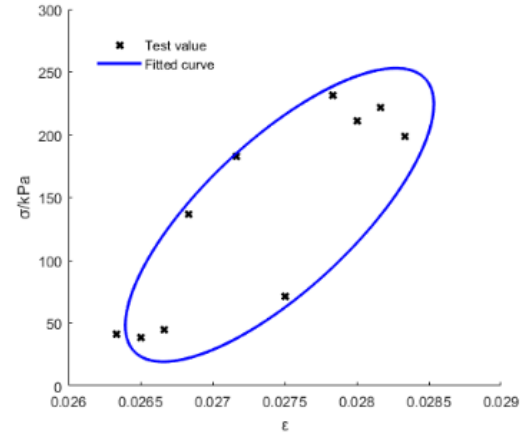

(**a**)

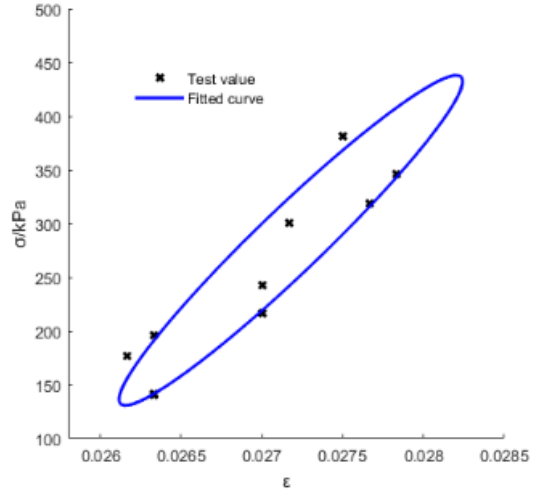

(**b**)

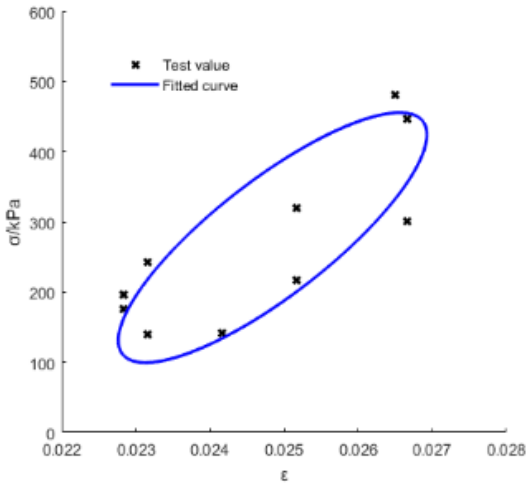

(**c**)

Figure 11. Tested and fitted hysteretic curves of the S2 specimen under different average stress: (**a**) 0.1 Mpa; (**b**) 0.2 Mpa; and (**c**) 0.3 Mpa.

Table 5. Area of hysteretic circle (A) for different CGS specimens (unit: N·m/m^3).

No.	σ_a/MPa	0.1			0.2			0.3		
	f/Hz	1	2	3	1	2	3	1	2	3
	S1	97.26	96.45	96.02	201.54	198.61	193.21	298.45	284.25	280.62
	S2	187.36	184.56	183.27	387.58	385.12	376.31	572.54	568.14	557.10
	S3	243.95	236.57	230.47	497.66	485.74	472.96	740.57	724.65	719.45

2.2.4. Determination of Creep–Fatigue Interaction Parameters

The creep–fatigue interaction parameters k and g can be determined by Equation (4) when the real part $J_r(t)$ and imaginary part $J_i(t)$ of the creep compliance $J(t)$ is calculated by substituting Equation (5) with Table 4 into Equation (2), and the real part $J_r(\omega)$ and imaginary part $J_i(\omega)$ of the fatigue compliance $J_i(\omega)$ is calculated by Equation (12). Tables 6–8 list the calculation results of creep and fatigue compliance for different gradations of CGS under different stress levels (σ_a).

Table 6. Calculation results of creep–fatigue interaction parameters k and g for different gradations of CGS (σ_a = 0.1 MPa).

No.	γ	f/Hz	Creep		Fatigue		Matrix(M)
			$J_r(t)$/Mpa^{-1}	$J_i(t)$/Mpa^{-1}	$J_r(\omega)$/Mpa^{-1}	$J_i(\omega)$/Mpa^{-1}	
S1	0.434	1	0.0157	0.000083	0.0531	0.001535	$\begin{pmatrix} 3.38 & 0 \\ 0 & 18.49 \end{pmatrix}$
		2	0.0157	0.000041	0.0530	0.001314	$\begin{pmatrix} 3.38 & 0 \\ 0 & 32.04 \end{pmatrix}$
		3	0.0157	0.000027	0.0532	0.001054	$\begin{pmatrix} 3.39 & 0 \\ 0 & 39.03 \end{pmatrix}$
S2	0.363	1	0.0328	0.000565	0.1143	0.006992	$\begin{pmatrix} 3.48 & 0 \\ 0 & 12.37 \end{pmatrix}$
		2	0.0328	0.000282	0.1145	0.005854	$\begin{pmatrix} 3.49 & 0 \\ 0 & 20.75 \end{pmatrix}$
		3	0.0328	0.000188	0.1142	0.004101	$\begin{pmatrix} 3.48 & 0 \\ 0 & 21.81 \end{pmatrix}$
S3	0.272	1	0.0611	0.001043	0.1754	0.013388	$\begin{pmatrix} 2.87 & 0 \\ 0 & 12.83 \end{pmatrix}$
		2	0.0611	0.000521	0.1756	0.009633	$\begin{pmatrix} 2.87 & 0 \\ 0 & 18.48 \end{pmatrix}$
		3	0.0611	0.000347	0.1758	0.005702	$\begin{pmatrix} 2.88 & 0 \\ 0 & 16.43 \end{pmatrix}$

Table 7. Calculation results of creep–fatigue interaction parameters k and g for different gradations of CGS (σ_a = 0.2 MPa).

No.	γ	f/Hz	Creep		Fatigue		Matrix(M)
			$J_r(t)$/Mpa^{-1}	$J_i(t)$/Mpa^{-1}	$J_r(\omega)$/Mpa^{-1}	$J_i(\omega)$/Mpa^{-1}	
S1	0.434	1	0.0135	0.000307	0.0512	0.002203	$\begin{pmatrix} 3.79 & 0 \\ 0 & 7.17 \end{pmatrix}$
		2	0.0135	0.000153	0.0513	0.002015	$\begin{pmatrix} 3.79 & 0 \\ 0 & 13.16 \end{pmatrix}$
		3	0.0135	0.000102	0.0512	0.001674	$\begin{pmatrix} 3.79 & 0 \\ 0 & 16.41 \end{pmatrix}$
S2	0.363	1	0.0282	0.000655	0.1282	0.011689	$\begin{pmatrix} 4.54 & 0 \\ 0 & 17.84 \end{pmatrix}$
		2	0.0282	0.000328	0.1284	0.010494	$\begin{pmatrix} 4.55 & 0 \\ 0 & 31.99 \end{pmatrix}$
		3	0.0282	0.000218	0.1283	0.008829	$\begin{pmatrix} 4.55 & 0 \\ 0 & 40.50 \end{pmatrix}$
S3	0.272	1	0.0525	0.000940	0.2155	0.027809	$\begin{pmatrix} 4.10 & 0 \\ 0 & 29.58 \end{pmatrix}$
		2	0.0525	0.000471	0.2153	0.022021	$\begin{pmatrix} 4.09 & 0 \\ 0 & 46.75 \end{pmatrix}$
		3	0.0525	0.000313	0.2154	0.018344	$\begin{pmatrix} 4.10 & 0 \\ 0 & 58.61 \end{pmatrix}$

Table 8. Calculation results of creep–fatigue interaction parameters k and g for different gradations of CGS (σ_a = 0.3 MPa).

No.	γ	f/Hz	Creep		Fatigue		Matrix(M)
			$J_r(t)$/Mpa^{-1}	$J_i(t)$/Mpa^{-1}	$J_r(\omega)$/Mpa^{-1}	$J_i(\omega)$/Mpa^{-1}	
S1	0.434	1	0.0116	0.000259	0.0857	0.006082	$\begin{pmatrix} 7.38 & 0 \\ 0 & 23.48 \end{pmatrix}$
		2	0.0116	0.000129	0.0858	0.005106	$\begin{pmatrix} 7.38 & 0 \\ 0 & 39.58 \end{pmatrix}$
		3	0.0116	0.000086	0.0855	0.004116	$\begin{pmatrix} 7.37 & 0 \\ 0 & 47.86 \end{pmatrix}$
S2	0.363	1	0.0243	0.000684	0.1433	0.017303	$\begin{pmatrix} 5.89 & 0 \\ 0 & 25.29 \end{pmatrix}$
		2	0.0243	0.000342	0.1435	0.015152	$\begin{pmatrix} 5.90 & 0 \\ 0 & 44.30 \end{pmatrix}$
		3	0.0243	0.000228	0.1436	0.012881	$\begin{pmatrix} 5.90 & 0 \\ 0 & 56.49 \end{pmatrix}$
S3	0.272	1	0.0453	0.000997	0.2874	0.037071	$\begin{pmatrix} 6.34 & 0 \\ 0 & 37.18 \end{pmatrix}$
		2	0.0453	0.000498	0.2872	0.035391	$\begin{pmatrix} 6.34 & 0 \\ 0 & 71.06 \end{pmatrix}$
		3	0.0453	0.000332	0.2871	0.031228	$\begin{pmatrix} 6.33 & 0 \\ 0 & 94.06 \end{pmatrix}$

It can be seen that with the increasing frequency f that the real part $J_r(t)$ of creep compliance (representing the energy storage compliance) is unchanged while the imaginary part $J_i(t)$ (representing the energy dissipation compliance) is deceased, which is the same as analytic results [28]. With the decreasing pebble content γ, $J_r(t)$ is decreased but $J_i(t)$ is increased, since a smaller value of γ means a greater clay content of the CGS specimen and thus stronger rheological properties with more energy dissipation in one cycle.

Similarly, with the increase in frequency f, the real part $J_r(\omega)$ of fatigue compliance is unchanged while the imaginary part $J_i(\omega)$ is deceased. With the decrease in γ, $J_r(\omega)$ is decreased but $J_i(\omega)$ is increased.

Obviously, the creep–fatigue interaction parameter k (corresponding to $J_r(t)$ and $J_r(\omega)$) is also unchanged while g (corresponding to $J_i(t)$ and $J_i(\omega)$) is increased with the increase in frequency f. With the decrease in γ, k changes non-monotonically while g is increased.

3. Test Verification of the Creep–Fatigue Interaction Model

3.1. Prediction Method and Test Scheme

Take the creep–fatigue interaction deformation of CGS as an example (the fatigue–creep interaction deformation is vice versa): the strain–time (ε–t) curve can be calculated by the following steps: (1) calculate $J_r(t)$ and $J_i(t)$ by Equation (2) to obtain the ε_c–t curve; (2) calculate $J_r(\omega)$ and $J_i(\omega)$ by Equation (12) to obtain the ε_f–t curve; (3) according to the creep–fatigue interaction factors k and g in Tables 6–8 to calculate the creep–fatigue interaction ε–t curve.

To verify the validity of the calculated ε–t curve based on the new creep–fatigue interaction model, triaxial creep–fatigue interaction tests, triaxial fatigue–creep interaction tests and the triaxial multi-interaction of three gradations of CGS specimens (Table 1) were conducted by triaxial test system (Figure 5). Table 9 lists the loading conditions of creep–fatigue interaction tests for different gradations of CGS under the same confining pressure (0.2 MPa).

Table 9. Loading conditions for triaxial creep–fatigue tests.

No.	Loading Order (C-F Interaction)	Creep		Fatigue		
		σ_c/Mpa	Holding Time (t) /min	σ_a/Mpa	f/Hz	Cycle Number/N
S1	C-F	0.1/0.2/0.3	120	0.1/0.2/0.3	1	7200

S2	F-C	0.1/0.2/0.3	120	0.1/0.2/0.3	1	7200
S3	C-F-C-F	0.2	120	0.2	1	14,400

3.2. Results and Analysis

3.2.1. Triaxial Creep–Fatigue Interaction Deformation

Figure 12 shows the predicted and tested curves of creep–fatigue (C-F) interaction deformation for S1 specimens under different stress levels. It is seen that all creep curves (the first part of C-F interaction) and fatigue curves (the second part of C-F interaction) have three stages: (1) instantaneous deformation stage; (2) attenuation deformation stage; and (3) stable deformation stage. The predicted creep and fatigue curves are close to the tested curves, which can prove the validity of the new creep–fatigue interaction model. The difference between the predicted and tested fatigue curves might be caused by the impact effects of fatigue loads and the discreteness of geotechnical materials.

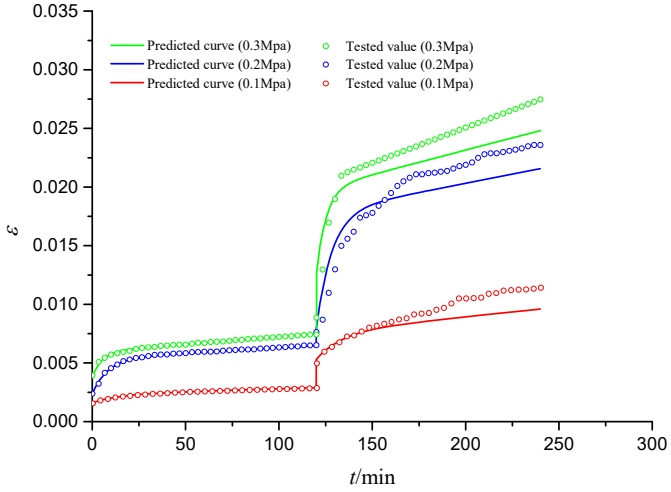

Figure 12. Predicted and tested curves of creep–fatigue interaction deformation (S1).

3.2.2. Triaxial Fatigue–Creep Interaction Deformation

Figure 13 shows the predicted and tested ε–t curves of fatigue–creep interaction for S2 specimens. It can be seen that all of the creep curves and all of the fatigue creep curves also have three deformation stages. In the fatigue stage, there is no situation in which the tested strain curve is much larger than the predicted strain curve compared with Figure 11, because the creep complex compliance is calculated based on the fatigue complex compliance and the predicted and tested curves are close to each other. In the creep stage, the predicted and tested curves are in good agreement. This again verifies the validity of the new creep–fatigue interaction model.

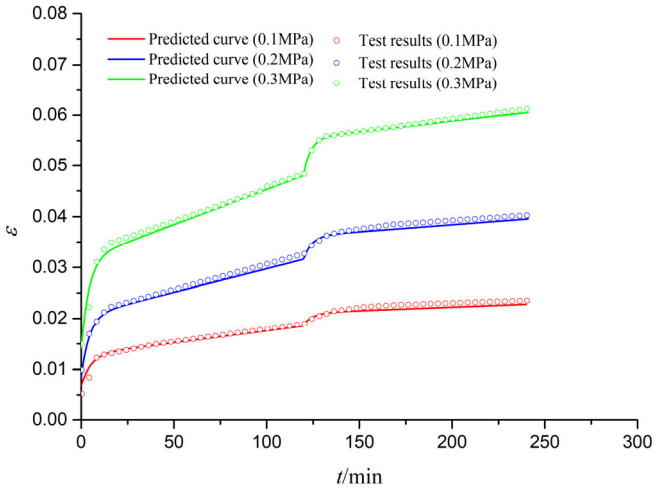

Figure 13. Predicted and tested curves of the fatigue–creep interaction deformation (S2).

3.2.3. Triaxial Creep–Fatigue Multi-Interaction Deformation

Figure 14 shows the predicted and tested curves of creep–fatigue multi-interaction for S3 specimen. It is seen that the predicted curves are in good agreement with the tested curves for two creep stages, while the predicted curves are larger than the tested curves for two fatigue stages. The reason is the dynamic load make a greater deformation for the same average stress. For the two fatigue stages, the strain produced from 120 min to 240 min is approximately 0.8%, while the strain produced from 360 min to 480 min is approximately 0.6%; the strain of the second fatigue stage is smaller than that of the first fatigue stage, because the rough pores of the CGS have been irreversibly reduced in the first fatigue stage, and after the first fatigue stage, the internal particles of the CGS will form a more stable force chain; hence, the strain generated in the second fatigue stage is less than the first fatigue stage.

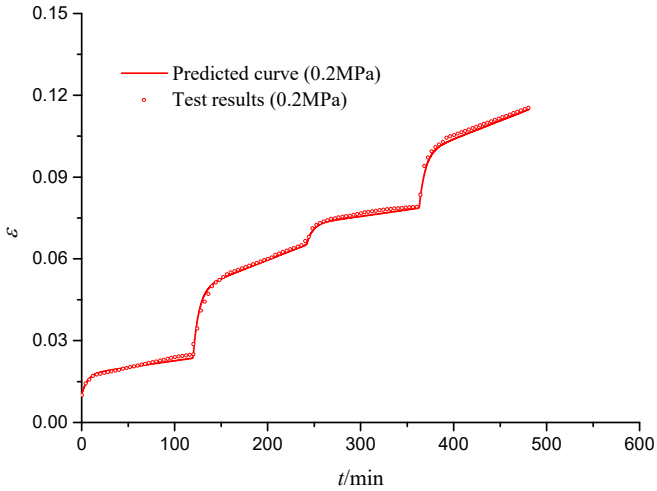

Figure 14. Predicted and tested curves of fatigue–creep multi-interaction deformation (S3).

4. Conclusions

(1) New transformation parameters (k and g) are proposed to establish a new creep–fatigue interaction model based on both the rheologic mechanics and the interactive relationship between creep and fatigue complex compliance, in order to predict the creep–fatigue interaction deformation of CGS.

(2) The creep–fatigue interaction factor k is almost unchanged with the frequency (f) and changed non-monotonic with the pebble content (γ). The creep–fatigue interaction factor g is increased with both f and γ. The creep strain and fatigue strain of the creep–fatigue and fatigue–creep interaction are increased with the increase in average stress (σ_a)
(3) For the different interaction orders (creep–fatigue interaction or fatigue–creep interaction), the fatigue deformation is always larger than the creep deformation under the same stress level because of the dynamic effect.
(4) For the creep–fatigue multi-interaction, the second creep and fatigue deformation is always smaller than the first creep and fatigue deformation because of the compaction effect.
(5) The new creep–fatigue interaction model is proved valid by the good agreement between the predicted results and test results of the triaxial creep–fatigue interaction. It can be further developed for predicting the creep–fatigue interaction of multi-layered coarse-grained soil.

Author Contributions: Conceptualization, J.Z. and Q.R.; data curation, J.Z.; funding acquisition, Q.R.; methodology, J.Z. and W.Y.; project administration, Q.R.; supervision, Q.R. and W.Y.; validation, J.Z. and Q.R.; writing—original draft, J.Z.; writing—review and editing, Q.R., and W.Y. All authors have read and agreed to the published version of the manuscript.

Funding: This research was funded by National Natural Science Foundation of China, grant number 51274251

Institutional Review Board Statement: Not applicable.

Informed Consent Statement: Not applicable.

Data Availability Statement: Not applicable.

Acknowledgments: This work was supported by the National Natural Science Foundation of China (grant number 51274251).

Conflicts of Interest: The authors declare that they have no known competing financial interests or personal relationships that could have appeared to influence the work reported in this paper.

References

1. *GB/T 50145—2007*; Standard for Engineering Classification of Soil. Planning Press: Beijing, China, 2008.
2. Medley, E. The Engineering Characterization of Mélanges and Similar Block-In-Matrix Rocks (Bimrocks). Ph.D. Thesis, University of California, Los Angeles, CA, USA, 1994.
3. Guo, G.Q. *Engineering Characteristics and Application of Coarse-Grained Soil*; The Yellow River Water Conservancy Press: Zhengzhou, China, 1998.
4. Long, X.; Cen, G.; Cai, L.; Chen, Y. Model experiment of uneven frost heave of airport pavement structure on coarse-grained soils foundation. *Constr. Build. Mater.* **2018**, *188*, 372–380. https://doi.org/10.1016/j.conbuildmat.2018.08.100.
5. Su, Y.; Cui, Y.-J.; Dupla, J.-C.; Canou, J.; Qi, S. A fatigue model for track-bed materials with consideration of the effect of coarse grain content. *Transp. Geotech.* **2020**, *23*, 100353. https://doi.org/10.1016/j.trgeo.2020.100353.
6. Cai, Y.; Chen, Y.; Cao, Z.; Sun, H.; Guo, L. Dynamic responses of a saturated poroelastic half-space generated by a moving truck on the uneven pavement. *Soil Dyn. Earthq. Eng.* **2015**, *69*, 172–181. https://doi.org/10.1016/j.soildyn.2014.10.014.
7. Manoukas, G.; Athanatopoulou, A.; Avramidis, I. Multimode pushover analysis for asymmetric buildings under biaxial seismic excitation based on a new concept of the equivalent single degree of freedom system. *Soil Dyn. Earthq. Eng.* **2012**, *38*, 88–96. https://doi.org/10.1016/j.soildyn.2012.01.018.
8. Hou, F.; Lai, Y.; Liu, E.; Luo, H.; Liu, X. A creep constitutive model for frozen soils with different contents of coarse grains. *Cold Reg. Sci. Technol.* **2018**, *145*, 119–126. https://doi.org/10.1016/j.coldregions.2017.10.013.
9. Larue, G.S.; Watling, C.N.; Black, A.; Wood, J.M. Improving the safety of distracted pedestrians with in-ground flashing lights. A railway crossing field study. *J. Saf. Res.* **2021**, *77*, 170–181. https://doi.org/10.1016/j.jsr.2021.02.014.
10. Liu, X.; Zhang, X.; Wang, H.; Jiang, B. Laboratory testing and analysis of dynamic and static resilient modulus of subgrade soil under various influencing factors. *Constr. Build. Mater.* **2019**, *195*, 178–186. https://doi.org/10.1016/j.conbuildmat.2018.11.061.
11. Liu, H.; Yang, X.; Jiang, L.; Lv, S.; Huang, T.; Yang, Y. Fatigue-creep damage interaction model of asphalt mixture under the semi-sine cycle loading. *Constr. Build. Mater.* **2020**, *251*, 119070. https://doi.org/10.1016/j.conbuildmat.2020.119070.
12. Wang, J.; Li, J.; Shi, Z. Deformation damage and acoustic emission characteristics of red sandstone under fatigue–creep interaction. *Theor. Appl. Fract. Mech.* **2022**, *117*, 103192. https://doi.org/10.1016/j.tafmec.2021.103192.

13. Ma, L.; Wang, Y.; Wang, M.; Xue, B.; Duan, L. Mechanical properties of rock salt under combined creep and fatigue. *Int. J. Rock Mech. Min. Sci.* **2021**, *141*, 104654. https://doi.org/10.1016/j.ijrmms.2021.104654.
14. Dong, N.; Wang, D.; Zhang, S.; Chen, Z.; Liang, H.; Ni, F.; Yu, J.; Yu, H. Exploring creep and recovery behavior of hot mix asphalt field cores with multi-sequenced repeated load test. *Constr. Build. Mater.* **2021**, *279*, 122435. https://doi.org/10.1016/j.conbuildmat.2021.122435.
15. Golub, V.P. Procedure for the calculation of cyclic creep and longevity from static loading data. *Int. Appl. Mech.* **1984**, *20*, 363–368. https://doi.org/10.1007/BF00882808.
16. Li, Y.; Sun, H.; He, X.; Tan, Y. Fatigue damage and creep characteristics of cement emulsified asphalt composite binder. *Constr. Build. Mater.* **2020**, *234*, 117416. https://doi.org/10.1016/j.conbuildmat.2019.117416.
17. Li, Q.; Liu, M.; Lu, Z.; Deng, X. Creep Model of High-Strength High-Performance Concrete Under Cyclic Loading. *J. Wuhan Univ. Technol. Sci. Ed.* **2019**, *34*, 622–629. https://doi.org/10.1007/s11595-019-2096-9.
18. Al-Mistarehi, B.W.; Khadaywi, T.S.; Hussein, A.K. Investigating the effects on creep and fatigue behavior of asphalt mixtures with recycled materials as fillers. *J. King Saud Univ.-Eng. Sci.* **2021**, *33*, 355–363. https://doi.org/10.1016/j.jksues.2020.09.004.
19. Tarefder, R.; Faisal, H.; Barlas, G. Freeze-thaw effects on fatigue LIFE of hot mix asphalt and creep stiffness of asphalt binder. *Cold Reg. Sci. Technol.* **2018**, *153*, 197–204. https://doi.org/10.1016/j.coldregions.2018.02.011.
20. Li, X.; Qi, C.; Zhang, P. A micro-macro confined compressive fatigue creep failure model in brittle solids. *Int. J. Fatigue* **2020**, *130*, 105278. https://doi.org/10.1016/j.ijfatigue.2019.105278.
21. Kindrachuk, V.M.; Thiele, M.; Unger, J. Constitutive modeling of creep-fatigue interaction for normal strength concrete under compression. *Int. J. Fatigue* **2015**, *78*, 81–94. https://doi.org/10.1016/j.ijfatigue.2015.03.026.
22. Gedik, A.; Selcuk, S.; Lav, A.H. Investigation of recycled fluorescent lamps waste as mineral filler in highway construction: A case of asphaltic pavement layers. *Resour. Conserv. Recycl.* **2021**, *168*, 105290. https://doi.org/10.1016/j.resconrec.2020.105290.
23. Alghrafy, Y.M.; Alla, E.-S.M.A.; El-Badawy, S.M. Rheological properties and aging performance of sulfur extended asphalt modified with recycled polyethylene waste. *Constr. Build. Mater.* **2021**, *273*, 121771. https://doi.org/10.1016/j.conbuildmat.2020.121771.
24. Delfosse-Ribay, E.; Djeran-Maigre, I.; Cabrillac, R.; Gouvenot, D. Comparison of Creep Behaviour and Fatigue Behaviour of Grouted Sand. *Soils Found.* **2007**, *47*, 185–194. https://doi.org/10.3208/sandf.47.185.
25. Ameli, A.; Babagoli, R.; Asadi, S.; Norouzi, N. Investigation of the performance properties of asphalt binders and mixtures modified by Crumb Rubber and Gilsonite. *Constr. Build. Mater.* **2021**, *279*, 122424. https://doi.org/10.1016/j.conbuildmat.2021.122424.
26. Qin, W.Z.; Wang, K.L. Research on the relationship between dynamic and static parameters of soil layer based on viscoelastic model. In Proceedings of the Fifteenth National Conference on Structural Engineering (No.II), 2006; pp. 307–310. Available online: https://kns.cnki.net/kcms/detail/detail.aspx?FileName=LXFY200610002066&DbName=CPFD2006 (accessed on 13 April 2022).
27. Yang, T.Q. *Theory of Viscoelasticity*; Huazhong University of Technology Press: Wuhan, China, 1992.
28. Li, H. *Viscoelastic Mechanical Response Analysis of Asphalt Mixture and Asphalt Pavement under Dynamic and Static*; Loads. Jilin University: Changchun, China, 2021.